Photonic Tuning of the Emission Color of Nanophosphor Films Processed at High Temperature

Dongling Geng, Gabriel Lozano, Mauricio E. Calvo, Nuria O. Núñez, Ana I. Becerro, Manuel Ocaña, and Hernán Míguez**

Photonics offers new possibilities to tailor the photoluminescence process in phosphor-converted light emitting diodes. Herein, it is demonstrated that the emission color of thin layers of rare-earth doped nanocrystals can be strongly modulated in tunable spectral ranges using optical resonators specifically designed to this end. $GdVO_4$:Dy^{3+} nanoparticles of controlled size and shape are synthesized using a solvothermal method with which highly transparent nanophosphor thin films are prepared. This paper designs and fabricates optical multilayers, which are transparent in the UV and resonant at the frequencies where the Dy^{3+} ions emit, to prove that the color coordinates of this emitter can be tuned from green to blue or yellow with unprecedented precision. Key to the achievement herein reported is the careful analysis of the structural and optical properties of thin nanophosphor layers with the processing temperature in order to achieve efficient photoluminescence while preserving the transparency of the film. The results open a new path for fundamental and applied research in solid-state lighting in which photonic nanostructures allow controlling the emission properties of state-of-the-art materials without altering their structure or chemical composition.

1. Introduction

The most widely employed route to generate artificial light is based on the use of high-efficiency UV or blue light-emitting diodes (LEDs) where part of the emission is converted to the visible by means of photoluminescent materials.[1,2] Among the different compounds employed for photoluminescence, rare-earth (RE)-doped crystals, so-called RE phosphors, have been extensively studied over the last decades.[3–9] In contrast to other luminescent materials, RE phosphors do not suffer from photobleaching, unlike fluorophore molecules, or from surface recombination and carrier diffusion issues present in semiconductor nanocrystals.[10] On top of this, RE phosphors feature low toxicity due to the absence of Pb or Cd, all of which make them ideal candidates for photoluminescence in LEDs. Nevertheless, despite the excellent optical properties and remarkable thermal and chemical stability, color tuning in RE phosphors is hard to achieve through the modification of their intrinsic material properties or excitation wavelength, which limits the color quality of LEDs.[11] Indeed, although routes based on a mixture of different RE ions doping different matrices or the combination of several RE ions codoping a given matrix have been explored for color adjustment, white light generated by these methods generally suffers from reabsorption or poor color stability since different emitting materials may exhibit distinct thermal quenching behavior and different aging rate.[12–16] An alternative route to tailor the emission of luminescent materials consists on the use of resonant photonic nanostructures.[17–25] However, to date standard phosphors have barely benefited from nanophotonics since, in general, they are clusters of micrometer-sized crystals and thus opacity is unavoidable due to significant light scattering. This scenario has recently changed. Phosphors with particle sizes smaller than 100 nm and controlled shapes opened the door to large-scale and low-cost fabrication of versatile transparent emitting thin films based on RE-doped nanocrystals.[26] In particular, techniques such as screen printing, dip coating, and electrophoretic methods combined with high-temperature annealing or cold isostatic pressing have been reported to achieve transparent nanophosphor films with thicknesses on the order of the micrometer,[27–33] which enable the development of photonic-based strategies to mold the photoluminescence process that seek to be herein investigated.

In this article, we demonstrate that optical resonators allow tailoring the color hue of nanophosphor thin films, opening a route toward the development of new types of photoluminescence layers. Among those RE ions that are attractive for the realization of white light emission in a single phase host,[34] Dy^{3+}-doped materials are interesting because they show two emission bands in the blue and yellow spectral regions,[35] being the intensity of the latter tunable through a careful selection of the inorganic host in which Dy^{3+} ions are incorporated.[36–39] In particular we make use of $GdVO_4$ as an inorganic host since this matrix provides the phosphor with chemical stability and large absorption cross section in the UV.[40,41] A solvothermal method is employed

Dr. D. Geng, Dr. G. Lozano, Dr. M. E. Calvo,
Dr. N. O. Núñez, Dr. A. I. Becerro, Prof. M. Ocaña,
Prof. H. Míguez
Institute of Materials Science of Seville (CSIC-US)
Américo Vespucio 49, 41092 Seville, Spain
E-mail: g.lozano@csic.es; h.miguez@csic.es

DOI: 10.1002/adom.201700099

to synthesize $GdVO_4$:Dy^{3+} nanoparticles of controlled size and shape. We find the experimental conditions to process these nanophosphors in the shape of films of controlled thickness with excellent optical properties. To do this, different material properties including surface morphology, optical transparency, along with the static and dynamic photoemission spectra of RE films annealed at different temperatures are evaluated. As a result, we find the sintering conditions that yield nanophosphor coatings emitting most efficiently while preserving transparency. Finally, a series of photonic multilayers made of ZrO_2 and SiO_2 that integrate such nanophosphor films as optical cavities are designed and fabricated using solution processing techniques. Tuning the lattice parameter of the photonic multilayer allows tailoring the color of the photoemission of the Dy^{3+} nanophosphor from green to blue or yellow with unprecedented precision.

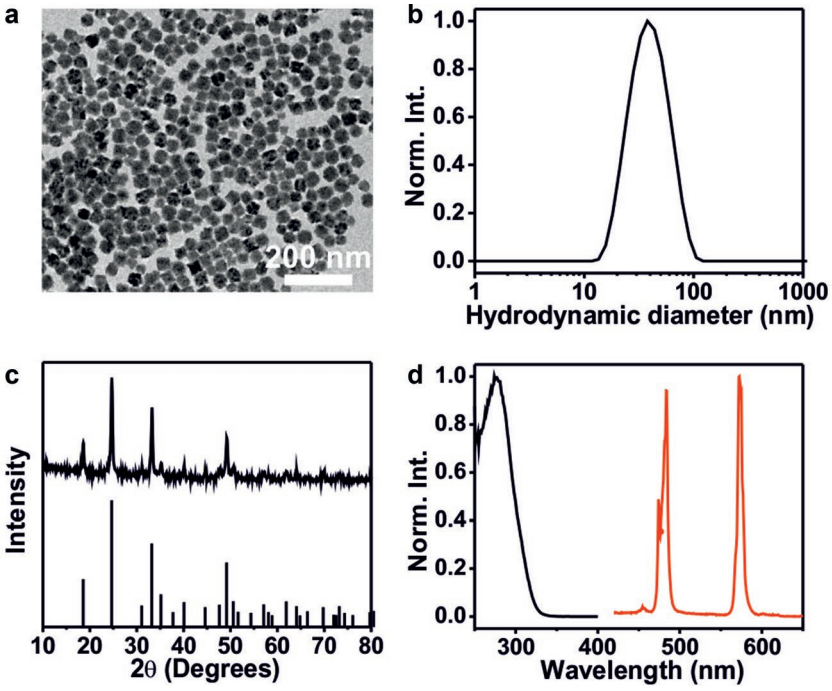

Figure 1. a) Transmission electron microscopy image and b) size distribution of $GdVO_4$:Dy^{3+} nanoparticles dispersed in methanol. c) X-ray diffraction pattern of dried $GdVO_4$:Dy^{3+} powder. Standard PDF 86-0996, ICDD 2014 is also shown for comparison. d) Excitation (black) and emission (red) spectra of the nanophosphors in methanol.

2. Results and Discussion

Figure 1a shows the transmission electron microscopy (TEM) image of the as-synthesized $GdVO_4$:Dy^{3+} nanophosphors (see the Experimental Section). Nanoparticles are almost equiaxial with an average diameter of 35 ± 5 nm, which is in excellent agreement with the average hydrodynamic diameter (37 ± 13 nm) obtained from dynamic light scattering measurements (Figure 1b). According to the X-ray diffraction (XRD) pattern displayed in Figure 1c, nanophosphors crystallize into the tetragonal $GdVO_4$ structure (PDF 86-0996, ICDD 2014), being 32 nm the crystallite size estimated using the Scherrer formula. These results indicate that nanocrystals present a single crystal character and that they do not aggregate when methanol is used as dispersant. Figure 1d shows the excitation (black line) and emission (red line) spectra of $GdVO_4$:Dy^{3+} nanocrystals dispersed in methanol. The excitation spectrum consists of an intense broad band centered at $\lambda = 276$ nm, which can be attributed to the charge transfer from the oxygen ligands to the central vanadium atom inside the VO_4^{3-} groups.[42] Lines associated to the direct excitation of Dy^{3+} ions cannot be observed because the absorption cross section of the *f*–*f* transitions for the Dy^{3+} is significantly small compared to that of the VO_4^{3-} groups, which suggests that the excitation of the Dy^{3+} is mainly due to the energy transfer from VO_4^{3-} groups to Dy^{3+} cations. The emission spectrum features two narrow bands upon excitation with UV light (λ = 276 nm): a blue band centered at λ = 483 nm that originates from the magnetic dipole transition between $^4F_{9/2}$–$^6H_{15/2}$, and a yellow band at λ = 572 nm from the hypersensitive electric dipole $^4F_{9/2}$–$^6H_{13/2}$ transition. No emission from the VO_4^{3-} groups is detected as expected,[43] confirming the efficient energy transfer from the VO_4^{3-} group to Dy^{3+} ions.

In order to prepare nanophosphor thin films, $GdVO_4$:Dy^{3+} nanoparticles dispersed in methanol are used as precursor suspensions for the spin-coating process. This alcohol is chosen because, as we mentioned before, no aggregation is observed in the suspension as shown in Figure 1a, and at the same time, films are obtained in few seconds during spin-coating. The adhesiveness of nanophosphors to the quartz substrate was improved by the previous deposition of a thin layer of ZrO_2 between the phosphor layer and the quartz substrate. **Figure 2**a displays a top view image of a nanophosphor film as prepared, showing that full coverage of the substrate is attained. An image of the cross section of such film reveals the different texture of the layers prepared, and demonstrates the uniformity of both ZrO_2 and $GdVO_4$:Dy^{3+} layers with thicknesses of 32 and 405 nm, respectively, as shown in Figure 2b. We characterize the surface topography of the films using atomic force microscopy (AFM): Figure 2c displays a 2D map of the surface of the film, whereas Figure 2d shows a topographic profile along the line depicted in Figure 2c. The analysis indicates that the films consist of closely packed particles, being the layers highly uniform with a root mean square roughness (R_{rms}) of 4 nm. Since the emission intensity of nanophosphors is limited by the low quantum yield that nanocrystals typically feature due to low crystallinity and large surface to volume ratio,[43] $GdVO_4$:Dy^{3+} nanophosphor films were subjected to a postannealing process in order to mitigate this effect. Figure 2e,f shows a top view and a cross section image of a nanophosphor film after annealing at 850 °C during 30 min. The particle size of $GdVO_4$:Dy^{3+} increases upon annealing at 850 °C together with the crystallite size estimated by XRD (79 nm), while the thickness of the layer decreased to 305 nm due to a densification of the film (Figure S1, Supporting Information). High temperature annealing yields optically flat crack-free layers, as the surface profile analysis, presented in Figure 2h,i, indicates

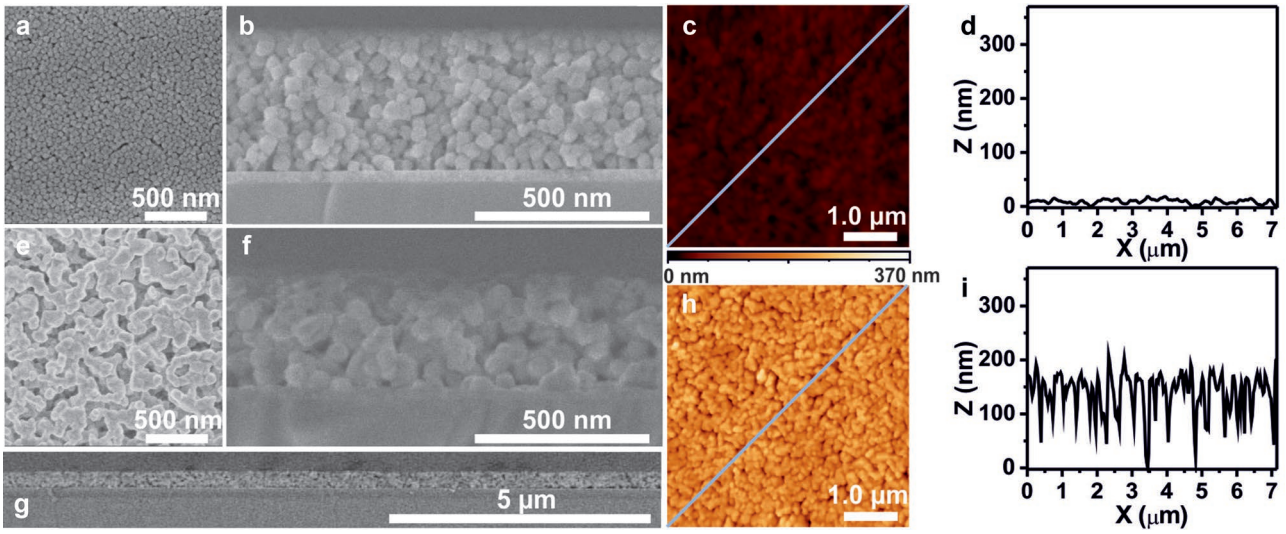

Figure 2. a,b) Scanning electron microscope (SEM) image of a top view (a) and a cross section of a $GdVO_4$:Dy^{3+} film as deposited at room temperature (RT). c) Atomic force microscope (AFM) topography of the surface of the nanophosphor film as deposited at RT. d) Height profile along the line depicted in (c). e–g) SEM image of a top view (e) and cross section with high (f) and low (g) magnification of a $GdVO_4$:Dy^{3+} film annealed at 850 °C. h) AFM topography of the surface of the film annealed at 850 °C. i) Height profile along the line depicted in (h).

($R_{rms} \approx 39$ nm that is significantly smaller than the wavelength of visible light). Results from the structural characterization of films annealed at 400 and 1000 °C are provided in the Supporting Information (Figure S2). As shown in the low magnification cross section image presented in Figure 2g, layers of uniform thickness over large areas are attained after high temperature treatment. Our results demonstrate that, due to the ability of the nanocrystals to form a uniform layer and their limited growth upon annealing, the high temperature processing does not alter the structural, and therefore optical, quality of the films. Notice that there are not so many examples of nanostructures that endure temperatures as high as 850 °C and can be still integrated in photonic devices.[44]

A spectroscopic analysis of the light reflected and transmitted by nanophosphor films annealed at different temperatures is performed in order to assess their transparency. **Figure 3**a shows the spectral dependence of the ballistic transmittance (T_B, defined as the fraction of the incident light transmitted in the incoming direction) of the nanophosphor films along with that of a quartz substrate and a quartz substrate coated with a thin ZrO_2 layer, which are also displayed in Figure 3a for referencing purposes. Specular reflectance spectra of such nanophosphor layers are shown in Figure S3 (Supporting Information). Nanophosphor films exhibit lower transmittance than the reference layers especially in the short wavelength range due to the absorption of VO_4^{3-} groups in the UV region. Intensity fluctuations that arise from the interference between light reflected and transmitted through the different interfaces of the system, which is a clear signal of the high optical quality of the films fabricated, are observable in all films annealed up to 700 °C. As the annealing temperature increases, the transmittance of the films reduces while spectral features fade, until they vanish for layers annealed at 1000 °C. Figure 3b displays the transparency, defined as $\int_{250}^{800} T_B(\lambda)d\lambda$, of the nanophosphor layers as a function of temperature. Notice that a transparency value of 100% corresponds to a medium through which light goes through without being scattered. Black symbols displayed in Figure 3b show that transparency is close to 90% and remains almost constant from RT to 700 °C, whereas the material becomes diffusive for temperature treatments above 850 °C. Indeed, the temperature dependence of the transparency can be well explained looking how the estimated $GdVO_4$:Dy^{3+} crystallite size varies with temperature (see red symbols in Figure 3b): it remains almost constant from 32 nm at RT to 36 nm at 700 °C and then grows up to 91 nm at 900 °C and to over 100 nm for higher temperatures. Such rise in the crystallite size can be correlated with a grain size growth that leads to an increase in the scattering strength of the films, which lessens T_B and consequently the transparency of the nanophosphor coatings, as shown in Figure 3b. In order to evaluate the performance of these layers for photoluminescence, it is also necessary to study how efficiently these films absorb the UV wavelength with which the nanophosphors are excited. Black symbols in Figure 3c shows the thermal treatment dependence of the fraction of light absorbed by the films at $\lambda = 276$ nm, where the VO_4^{3-} group absorbs, as shown in Figure 1d. Our measurements indicate that the absorptance decreases gradually from 80% for films annealed at 400 °C to 60% for films at 1000 °C. This originates from the enlargement of the nanocrystal size with temperature, which causes a larger fraction of the incident light to be scattered, as confirmed by the diffuse transmittance measurements displayed as red symbols in Figure 3c. Finally, Figure 3d shows digital camera pictures taken from a film as deposited and films annealed at 700 and 850 °C, which bring to light the high optical quality of the nanophosphor layers developed and processed up to those temperatures.

An analysis of both the static and dynamic photoluminescence (PL) of the fabricated $GdVO_4$:Dy^{3+} layers is also performed. **Figure 4**a shows the annealing temperature dependence of the PL intensity-integrated between 420 and 650 nm of nanophosphor films excited at $\lambda = 276$ nm. The different PL spectra are shown in Figure S4 (Supporting Information). It can be observed that the spectral position of the PL peaks remains unchanged with the

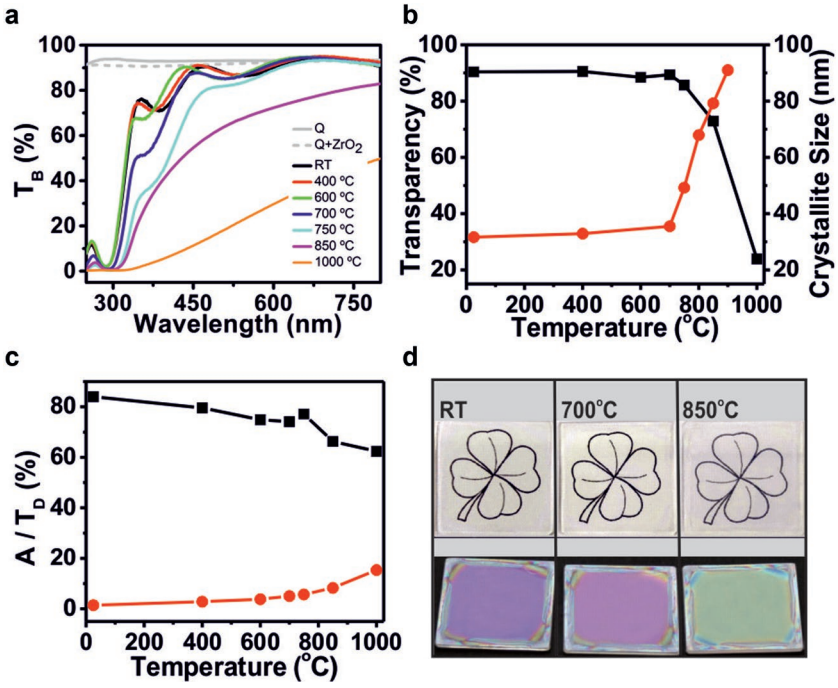

Figure 3. a) Spectral dependence of the ballistic transmittance (T_B) of $GdVO_4$:Dy^{3+} nanophosphor films deposited over a ZrO_2 coated quartz substrate as prepared (black) and annealed at 400 °C (red), 600 °C (green), 700 °C (blue), 750 °C (cyan), 850°C (magenta), and 1000 °C (orange). We also show T_B for a quartz substrate (gray) and a 35 nm thick ZrO_2 layer (dashed gray). b) Annealing temperature dependence of the transparency (black symbols) and crystallite size (red symbols) of nanophosphor films. Lines are only guides to the eye. c) Annealing temperature dependence of the fraction of light absorbed (A, black symbols) and diffusely transmitted (T_D, red symbols) by the nanophosphor films. Lines are only guides to the eye. d) Digital pictures of light reflected under daylight from nanophosphor films on quartz placed over a white paper in which a flower is sketched in a direction close to the normal to the surface (upper panels), and over a black paper at an oblique angle (lower panels).

annealing temperature. Regarding PL intensity, three different regions can be identified in the plot: (i) it increases with temperature treatments up to 700 °C, (ii) it plateaus between 700 and 800 °C, and finally, (iii) the intensity shows a reduction for temperatures higher than 800 °C. In order to shed some light on the physical origin of this behavior, we perform an analysis of the decay dynamics of the nanophosphor PL. To illustrate this, Figure 4b displays decay curves of the $^4F_{9/2}$ level of Dy^{3+} activators monitored at $\lambda = 572$ nm under excitation at $\lambda = 276$ nm for the films as prepared and annealed at 400, 700, and 900 °C. A double exponential model can be employed to fit the time-resolved PL measurements

$$\mathrm{PL}(t) = A_1 \mathrm{e}^{-t/\tau_1} + A_2 \mathrm{e}^{-t/\tau_2} \quad (1)$$

where τ_1 and τ_2 are the long and short decay components associated to the transition of Dy^{3+} cations that sit in the bulk or close to the surface of the nanoparticle, respectively, and A_1 and A_2 are the fitting constants. The average lifetime (τ) of $^4F_{9/2}$ electronic levels of $GdVO_4$:Dy^{3+} films heated at different temperatures can be calculated according to

$$\tau = \frac{\int t\mathrm{PL}(t)\,\mathrm{d}t}{\int \mathrm{PL}(t)\,\mathrm{d}t} = \frac{A_1\tau_1^2 + A_2\tau_2^2}{A_1\tau_1 + A_2\tau_2} \quad (2)$$

Fitting parameters along with the fitting curves are shown in Figure S5 and Table S1 (Supporting Information). Figure 4c shows that (i) τ increases from 163 µs at RT to 355 µs at 600 °C, and (ii) it decreases from 361 µs at 700 °C to 236 µs at 900 °C. Similar behavior is observed if integrated or time-resolved PL is monitored at $\lambda = 483$ nm, where the blue emission line of $GdVO_4$:Dy^{3+} sits. In general, thermal treatment causes the growth of the crystallite size, as we have already demonstrated, along with the removal of impurities adsorbed at the nanocrystal surface during the synthesis such as OH^- or polyacrylic acid (PAA), which act as quenchers of the emission.[43] Fourier transform infrared (FTIR) spectrum of $GdVO_4$:Dy^{3+} nanophosphors annealed at different temperatures are shown in Figure S6 (Supporting Information), which demonstrates that as the annealing temperature increases peaks associated to the presence of hydroxyl and carboxylate groups disappear. Consequently, annealed nanophosphors feature a reduced amount of structural defects and surface traps, which lessens the nonradiative decay rate of Dy^{3+}. This is in agreement with the $^4F_{9/2}$ lifetime rise observed in Figure 4c that leads to an improved quantum yield (from 2.6% at RT to 21.1% at 700 °C), which results in a higher PL intensity when the temperature increases from RT to 700 °C, as observed in Figure 4a. A further increment of the annealing temperature of the nanophosphors leads to a reduction of lifetime that can be attributed to an enlargement of the radiative decay rate. From 700 °C the crystallite size grows significantly, which may increase the effective refractive index of nanophosphor layers and therefore modify the local density of photonic states available for the decay of Dy^{3+} cations.[29,45–48] Such increase in the radiative decay leads to a slight increase of the PL between 700 and 800 °C, which may suggest a minor change in the quantum yield (from 21.1% at 700 °C to 25.1 at 800 °C). Interestingly, decay curves extracted from films annealed above 750 °C are fitted using a single exponential model (see Table S1, Supporting Information), which indicates that, as a result of crystallite growth combined with the removal of impurities adsorbed at the nanoparticle surface, from 750 °C different locations of the rare cations are indistinguishable. Annealing the films at temperatures above 850 °C produces a further decrease of the lifetime along with a reduction of the PL, as displayed in Figure 4a,c. Such depletion of the intensity can be attributed to the decrease in the fraction of UV light absorbed shown in Figure 3c along with a halt of the quantum yield of the system (25.9% at 900 °C). As it is our goal to find the experimental conditions under which to prepare nanophosphor coatings that are both transparent and bright, we focus on films annealed at 700 °C to continue with our study. In Figure 4d we present the PL intensity of films of different thickness. PL spectra are displayed in Figure S7 (Supporting

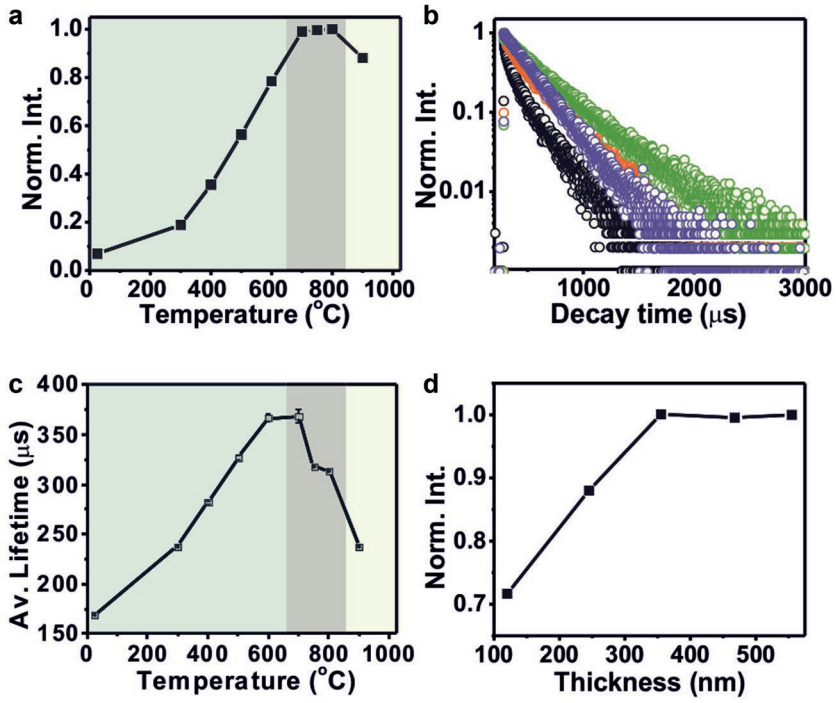

Figure 4. a) Annealing temperature dependence of the photoluminescence (PL) intensity of $GdVO_4$:Dy^{3+} nanophosphor films normalized to the PL of the film annealed at 700 °C. b) Time dependence PL of nanophosphor films as prepared (black) and annealed at 400 °C (red), 700 °C (purple), and 900 °C (green). c) Annealing temperature dependence of the average lifetime of the films. d) Film thickness dependence of the PL intensity of nanophosphor layers annealed at 700 °C normalized to the intensity of the thickest layer.

Information). PL increases with the amount of material up to a thickness of 350 nm, where the PL plateaus, meaning that such thickness is enough as to absorb the complete fraction of the incident light that is not reflected in the nanophosphor/air interface as it would be required if such films were integrated as photoluminescent materials in LEDs.

Once we have demonstrated bright $GdVO_4$:Dy^{3+} films with high optical quality, we aim at creating a photonic environment capable of modifying the emission spectrum of such nanophosphors. To achieve this, $GdVO_4$:Dy^{3+} nanocrystals are integrated in an resonator as an optical cavity between two multilayers that behave as dielectric mirrors in a broad spectral range that includes the emission lines of Dy^{3+} ions. The alternate dielectric layers of choice, made of SiO_2 and ZrO_2 nanoparticles, were selected due to (i) their compatibility with sequential solution processing, (ii) their refractive index contrast, which provides efficient broad band reflection with just a few alternate layers, and (iii) their transparency in the UV region for $\lambda > 200$ nm, a requirement to achieve efficient excitation of the emitters employed. The thickness of each layer in the resonator can be precisely determined through the deposition conditions, which allow an accurate control over the photon modes of the cavity. **Figure 5** shows cross section images of the resonators as prepared and thermally annealed at 700 °C. Scanning electron microscope (SEM) pictures reveal smooth and continuous interfaces between different types of layers with absence of interpenetration before and after heat treatment, which demonstrates that the structural quality of the complete ensemble is preserved after annealing. In fact, the use of nanoparticles both prevents the penetration of the porous nanophosphor layer and provides high thermal and mechanical stability to the ensemble. The porous nature of the nanoparticle-based films makes the optical properties of the photonic structure sensitive to environmental vapor pressure variations, as it has been investigated for other porous optical multilayers.[49]

The optical cavity breaks the translational symmetry of the 1D lattice, which gives rise to photonic modes to which the emission of the nanophosphors can couple. Such resonant modes are allowed states in the photonic pseudogap, which are signaled by dips in the reflectance spectrum of the resonator, being their spectral position defined by the lattice parameter of the multilayer and the thickness of the optical cavity (see Figure S8, Supporting Information). **Figure 6**a–d shows the reflectance and emission spectra upon excitation with $\lambda = 276$ nm of four resonators designed to exhibit resonant cavity modes matching the emission lines of the Dy^{3+}. Indeed, efficient coupling between light emitted by the nanophosphors and optical cavity modes is attained for those wavelengths in which spectral overlap between emission bands of Dy^{3+} and dips in the reflectance spectra occurs. As a consequence, the emitted light is funneled from the optical resonator, resulting in a PL directional enhancement due to an efficient out-coupling of the emitted light in the normal direction.[50] For the sake of comparison, we also show the emission spectrum of a reference layer consisting of a 340 nm thick $GdVO_4$:Dy^{3+} nanophosphor layer sandwiched between two ZrO_2 films of 60 and 10 nm, respectively. Emission spectra displayed in Figure 6a,c shows that

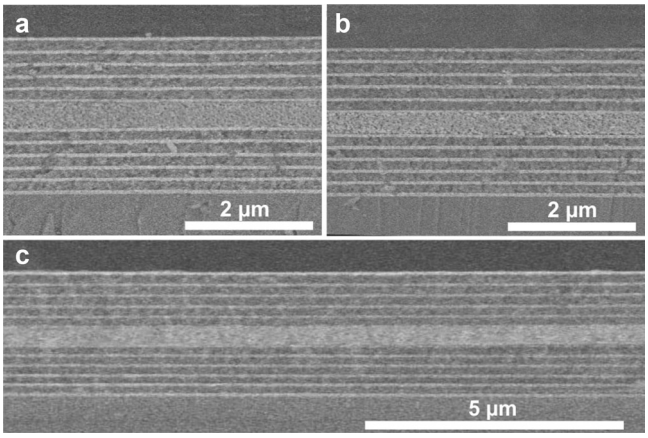

Figure 5. a) Scanning electron microscope (SEM) image of a cross section of a resonator in which the central layer of $GdVO_4$:Dy^{3+} is acting as an optical cavity. b) SEM image of the same resonator after annealing at 700 °C. c) Low magnification SEM picture of (b).

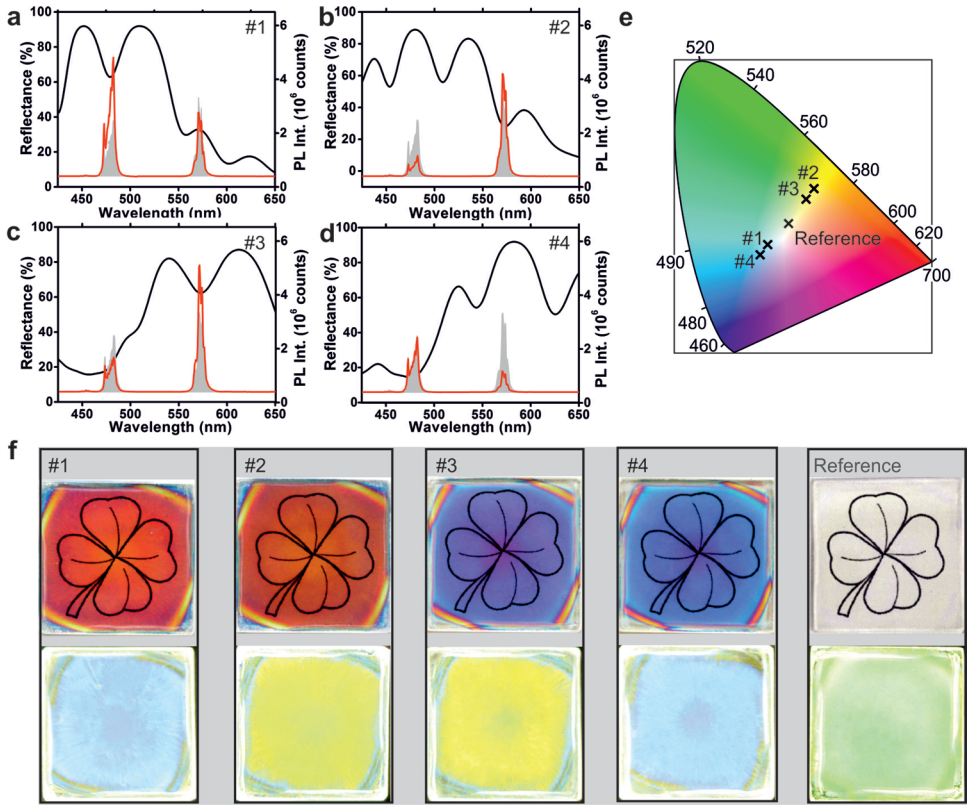

Figure 6. a–d) Reflectance (black) and photoluminescence (red) spectra obtained from $GdVO_4$:Dy^{3+}-containing optical resonators annealed at 700 °C built using dielectric multilayers made of five unit cells with structural parameters: SiO_2/ZrO_2: 95 nm/60 nm and $ZrO_2/GdVO_4/ZrO_2$: 80 nm/340 nm/10 nm, labeled as #1 (a), SiO_2/ZrO_2: 95 nm/60 nm and $ZrO_2/GdVO_4/ZrO_2$: 165 nm/340 nm/10 nm, labeled as #2 (b), SiO_2/ZrO_2: 125 nm/65 nm and $ZrO_2/GdVO_4/ZrO_2$: 80 nm/340 nm/10 nm, labeled as #3 (c), and SiO_2/ZrO_2: 125 nm/65 nm and $ZrO_2/GdVO_4/ZrO_2$: 165 nm/340 nm/10 nm, labeled as #4 (d). The emission of a reference sample consisting of a nanophosphor layer of similar thickness is also plotted in each panel with a gray curve that has been filled with the same color. e) CIE Chromaticity coordinates of the films whose response is shown in (a)–(d). f) Digital pictures taken under daylight of the light reflected by nanophosphor-containing multilayers over a white paper in which a flower is sketched (upper panels), and of the light emitted by the samples using a UV lamp to excite the Dy^{3+} cations (lower panels). Pictures under daylight are taken at an oblique angle to show it is possible to see through nanophosphor films.

we can enhance the blue (1.9-fold respect to the emission intensity of the reference blue line) or yellow line (1.5-fold) while keeping the other line, yellow or blue, respectively, almost unaltered. Analogously, Figure 6b,d shows that we can diminish the PL of the blue (0.3-fold) or yellow line (0.4-fold) while keeping the intensity of the complementary yellow or blue, respectively, barely unaffected. Our results demonstrate that the emission color of nanophosphor layers can be accurately tuned from green to blue or yellow as shown in the chromaticity diagram presented in Figure 6e. To exhibit a clear visual effect of the large tunability of the color coordinates of the Dy^{3+} ions attained when using an optical resonator, Figure 6f shows pictures, taken with a digital camera, of patent yellow and blue emission of transparent nanophosphor films embedded in photonic multilayers devised to this end. For the sake of comparison we also display the emission of the reference, which shows a green hue. To the best of our knowledge, our results constitute the first example of fine tuning of the spectral emission properties of single phase phosphor layers processed at high temperature by means that do not involve changing their chemical composition.

3. Conclusions

In summary, we have demonstrated that photonic nanostructures offer a new route to tailor the emission properties of nanophosphors accurately. We found the experimental conditions under which to prepare rare earth ion containing films that are bright and transparent. We synthesize $GdVO_4$:Dy^{3+} nanocrystals of controlled size and shape that we deposit as thin films. A thorough structural and optical characterization reveal that a post processing of the films at high temperature allows increasing the emission intensity of the nanophosphors by more than one order of magnitude while preserving their transparency, which enables their integration into optical resonators. A careful design of the structural parameters of such resonators to sustain photonic modes at the emission lines of Dy^{3+} cations allows tailoring the chromaticity of the emission with high precision. The combination of nanophotonics and nanophosphor materials pave the way for a new generation of optically active materials for integration in light-emitting devices of enhanced functionality and improved performance.

4. Experimental Section

Materials Preparation: Chemicals: Gadolinium(III) nitrate hexahydrate ($Gd(NO_3)_3{\cdot}6H_2O$, Aldrich, 99.9%), dysprosium(III) nitrate hydrate ($Dy(NO_3)_3{\cdot}xH_2O$, Aldrich, 99.9%), sodium orthovanadate (Na_3VO_4, Aldrich, 99.9%), PAA (average $M_w \approx 1800$, Aldrich), ethylene glycol (EG), zirconium (IV) *n*-propoxide 70% in 1-propanol (Aldrich), triblock copolymers Pluronic F127 ($M_w \approx 12\,600$), 2,4-Pentanedione (acetylacetonate, acac, AlfaAesar), SiO_2 (LUDOX TMA, Aldrich), polystyrene (Aldrich, 182427), toluene, absolute ethanol, methanol, HCl (3.571 mol L^{-1}, Panreac) and MilliQ water.

Nanophosphor Synthesis: For the $GdVO_4:Dy^{3+}$ nanophosphors synthesis, a method based on the facile solvothermal route described in ref. [43] was used. Suitable amounts of RE nitrates were dissolved in ethylene glycol (2.5 mL). The doping concentration of Dy^{3+} in the $GdVO_4$ host was fixed at 2% in molar ratio. To facilitate the dissolution of reagents in EG the solutions were mildly heated (≈80 °C) under magnetic stirring. In a separate vial, a weighted amount of Na_3VO_4 and 2 mg mL^{-1} of PAA were dissolved in an EG–H_2O mixture (1 mL EG + 1.5 mL H_2O). After cooling down to room temperature, both solutions were then admixed while keeping the magnetic stirring. In the final solutions, the total RE and the Na_3VO_4 concentrations were kept constant at 0.02 and 0.1 mol L^{-1}, respectively, whereas the final EG–H_2O volumetric ratio was 3.5:1.5. The as-prepared solutions were then aged for 3 h in tightly closed test tubes using an oven preheated at 120 °C. Then, the resulting dispersions were cooled down to room temperature, centrifuged to remove the supernatants, and washed twice with ethanol and once with distilled water. Finally, the precipitates were redispersed in methanol with a concentration of 5% by wt.

ZrO_2 Precursor Sol Synthesis: Sols were prepared following a synthesis reported elsewhere.[51] Briefly, a mix of ethanol, acac, zirconium *n*-propoxide, HCl, water and F127 in a molar ratio of 40:1:1:1:20:0.005 is prepared. Zirconium propoxide, acac, and F127 were dissolved in 80% of the total ethanol and the mixture was stirred for 1 min. HCl and water dissolved in the remaining ethanol were added dropwise while stirring to the first solution. The final sol was then stirred during 1 h.

Nanophosphor Layer Preparation: ZrO_2 films were deposited over a quartz substrate by spin-coating (Laurell WS-400) using 190 µL of the ZrO_2 precursor sol with an acceleration ramp of 11340 $rpms^{-1}$ and a final rotation speed of 3000 rpm. The film was annealed at 400 °C for 10 min. Then, a 120 nm thick layer of $GdVO_4:Dy^{3+}$ nanophosphors was deposited by spin-coating using 180 µL of nanophosphor dispersion with an acceleration ramp of 11340 $rpms^{-1}$ and a final rotation speed of 1500 rpm. In order to obtain layers of different thickness, several $GdVO_4:Dy^{3+}$ layers were deposited using the same deposition conditions. The as-prepared nanophosphor coatings were annealed at different temperatures (up to 1000 °C) for 30 min.

Optical Multilayer Preparation: Optical multilayers were fabricated by the alternated deposition of layers prepared with ZrO_2 precursor sol and SiO_2 nanoparticle suspension.[52] Polystyrene was employed to prevent the infiltration of the ZrO_2 precursors into the SiO_2 and the $GdVO_4:Dy^{3+}$ layers, which are inherently porous. The multilayer starts with the deposition of the ZrO_2 sol on top of a clean quartz substrate. This first layer was treated at 400 °C for 10 min. Next, a layer of SiO_2 nanoparticles was deposited on top of the ZrO_2 layer. After that, 180 µL of the polystyrene solution (0.5 wt% toluene solution) was spin-casted onto the preformed multilayer structure with an acceleration ramp of 11340 $rpms^{-1}$ and a final rotation speed of 3000 rpm. This process was repeated until five unit cells were deposited. Then, a nanophosphor layer sandwiched between two ZrO_2 layers was deposited to build an optical cavity. The multilayer was annealed at 700 °C for 30 min to provide the system with mechanical stability. Another five unit cells were deposited after the sample cooled down to room temperature. Finally, a layer of ZrO_2 was deposited to complete the photonic multilayer, which was annealed at 700 °C for 30 min again. For the sake of comparison, a $GdVO_4:Dy^{3+}$ nanophosphor layer sandwiched between two ZrO_2 layers annealed at the same temperature (700 °C) for 30 min was also prepared for referencing purpose.

Characterization: Structural Characterization: The crystalline structure of as-prepared nanophosphors was investigated by XRD (Panalytical X'pert Pro). The crystallite size was estimated from the most intense XRD peak of the $GdVO_4$ structure by using the Scherrer equation. The shape of the nanophosphor was examined by TEM (Philips 200CM). The particle size distributions were obtained from dynamic light scattering (Zetasizer Nano ZS90, Malvern). SEM images of the multilayer films deposited onto quartz were taken by using a microscope Hitachi S4800. The infrared spectra of the nanophosphors diluted in KBr pellets were recorded in a Jasco FT/IR-6200 Fourier transform infrared spectrophotometer.

Surface Characterization: The surface of the nanophosphor films was characterized by AFM (Park Systems XE-100) working at tapping mode.

Optical Characterization: The excitation and emission spectra as well as the lifetime of these samples were measured in a Horiba JobinYvon spectrofluorometer (Fluorolog FL3-11). Total reflectance, total transmittance, diffuse transmittance, ballistic reflectance, and ballistic transmittance were measured using a Cary 7000 series UV–vis–NIR spectrophotometer along with an integrating sphere attached to it. Quantum yield measurements were performed using a Hamamatsu C9920-02 QY. Excitation wavelength was fixed at 276 nm and the emission intensity was integrated in the spectral range comprised between 400 and 700 nm. Notice that reported values account for both the intrinsic yield of the Dy^{3+} and the efficiency of the energy transfer process between the vanadate group and the rare earth ion.

Supporting Information

Supporting Information is available from the Wiley Online Library or from the author.

Acknowledgements

The authors thank C. Momblona and H. Bolink for their help with QY measurements. Funding for the development of the research leading to these results was received from the European Research Council under the European Union's Seventh Framework Programme (FP7/2007–2013)/ERC Grant Agreement 307081 (POLIGHT) and the Spanish Ministry of Economy and Competitiveness under Grant No. MAT2014 54852-R. D.G. acknowledges the funding from the Marie Curie ActionMSCA-IF-2014-657434 corresponding to the European Union's Horizon 2020 Programme.

Conflict of Interest

The authors declare no conflict of interest.

Keywords

color tuning, nanophotonics, rare-earth nanocrystals, solid-state lighting

Received: February 1, 2017
Revised: March 20, 2017
Published online: May 22, 2017

[1] S. Pimputkar, J. S. Speck, S. P. DenBaars, S. Nakamura, *Nat. Photonics* **2009**, *3*, 180.
[2] J. Y. Tsao, M. H. Crawford, M. E. Coltrin, A. J. Fischer, D. D. Koleske, G. S. Subramania, G. T. Wang, J. J. Wierer, R. F. Karlicek Jr., *Adv. Opt. Mater.* **2014**, *2*, 809.

[3] H. A. Höppe, *Angew. Chem., Int. Ed.* **2009**, *48*, 3572.
[4] P. F. Smet, A. B. Parmentier, D. Poelman, *J. Electrochem. Soc.* **2011**, *158*, R37.
[5] C. C. Lin, R.-S. Liu, *J. Phys. Chem. Lett.* **2011**, *2*, 1268.
[6] T. M. Tolhurst, S. Schmiechen, P. Pust, P. J. Schmidt, W. Schnick, A. Moewes, *Adv. Opt. Mater.* **2016**, *4*, 584.
[7] W. Lv, Y. Jia, Q. Zhao, M. Jiao, B. Shao, W. Lü, H. You, *Adv. Opt. Mater.* **2014**, *2*, 183.
[8] P.-P. Dai, C. Li, X.-T. Zhang, J. Xu, X. Chen, X.-L. Wang, Y. Jia, X. Wang, Y.-C. Liu, *Light Sci. App.* **2016**, *5*, e16024.
[9] W. Cheng, F. Rechberg, M. Niederberger, *ACS Nano* **2016**, *10*, 24067.
[10] B. Guzelturk, P. L. H. Martinez, Q. Zhang, Q. Xiong, H. Sun, X. W. Sun, A. O. Govorov, H. V. Demir, *Laser Photonics Rev.* **2014**, *8*, 73.
[11] J. H. Oh, S. J. Yang, Y. R. Do, *Light Sci. App.* **2014**, *3*, e141.
[12] A. A. Setlur, W. J. Heward, M. E. Hannah, U. Happek, *Chem. Mater.* **2008**, *20*, 6277.
[13] Y. F. Liu, X. Zhang, Z. D. Hao, X. J. Wang, J. H. Zhang, *J. Mater. Chem.* **2011**, *21*, 6354.
[14] N. Kimura, K. Sakuma, S. Hirafune, K. Asano, N. Hirosaki, R.-J. Xie, *Appl. Phys. Lett.* **2007**, *90*, 051109.
[15] C. C. Lin, Y. S. Zheng, H. Y. Chen, C. H. Ruan, G. W. Xiao, R. S. Liu, *J. Electrochem. Soc.* **2010**, *157*, H900.
[16] A. J. Fernández-Carrión, M. Ocaña, J. García-Sevillano, E. Cantelar, A. I. Becerro, *J. Phys. Chem. C* **2014**, *118*, 18035.
[17] J. J. Wierer, A. David, M. M. Megens, *Nat. Photonics* **2009**, *3*, 163.
[18] O. Sánchez-Sobrado, M. E. Calvo, N. Núñez, M. Ocaña, G. Lozano, H. Míguez, *Nanoscale* **2010**, *2*, 936.
[19] L. Novotny, N. van Hulst, *Nat. Photonics* **2011**, *5*, 83.
[20] E. Matioli, S. Brinkley, K. M. Kelchner, Y. L. Hu, S. Nakamura, S. DenBaars, J. Speck, C. Weisbuch, *Light Sci. Appl.* **2012**, *1*, e22.
[21] S. Murai, M. A. Verschuuren, G. Lozano, G. Pirruccio, A. F. Koenderink, J. Gómez Rivas, *Opt. Mater. Express* **2012**, *2*, 1111.
[22] G. Lozano, D. J. Louwers, S. R. K. Rodriguez, S. Murai, O. T. A. Jansen, M. A. Verschuuren, J. Gómez Rivas, *Light Sci. Appl.* **2013**, *2*, e66.
[23] G. B. Akselrod, C. Argyropoulos, T. B. Hoang, C. Ciracì, C. Fang, J. Huang, D. R. Smith, M. H. Mikkelsen, *Nat. Photonics* **2014**, *8*, 835.
[24] A. F. Koenderink, A. Alù, A. Polman, *Science* **2015**, *348*, 516.
[25] G. Lozano, S. R. K. Rodriguez, M. A. Verschuuren, J. Gómez Rivas, *Light Sci. App.* **2016**, *5*, e16080.
[26] S. Gai, C. Li, P. Yang, J. Lin, *Chem. Rev.* **2014**, *114*, 2343.
[27] O.-H. Kim, H. Shin-Woo, J.-K. Lee, *ACS Nano* **2010**, *4*, 3397.
[28] W.-S. Song, K.-H. Lee, Y. R. Do, H. Yang, *Adv. Funct. Mater.* **2012**, *22*, 1885.
[29] G. Dantelle, B. Fleury, J.-P. Boilot, T. Gacoin, *ACS Appl. Mater. Interfaces* **2013**, *5*, 11315.
[30] A. Klausch, H. Althaues, T. Freudenberg, S. Kaskel, *Thin Solid Films* **2012**, *520*, 4297.
[31] Y. Iso, S. Takeshita, T. Isobe, *Langmuir* **2014**, *30*, 1465.
[32] W.-S. Song, K.-H. Lee, Y.-S. Kim, H. Yang, *Mater. Chem. Phys.* **2012**, *135*, 51.
[33] R. Kubrin, J. J. do Rosario, G. A. Schneider, *RSC Adv.* **2015**, *5*, 25555.
[34] M. Shang, C. Li, J. Lin, *J. Chem. Soc. Rev.* **2014**, *43*, 1372.
[35] G. Blasse, *Chemistry and Physics of R-Activated Phosphors. Handbook on the Physics and Chemistry of Rare-Earths*, Elsevier, Amsterdam, The Netherlands **1979**.
[36] Q. Su, Z. Pei, L. Chi, H. Zhang, Z. Zhang, F. Zou, *J. Alloys Compd.* **1993**, *192*, 25.
[37] P. S. Babu, P. P. Rao, S. K. Mahesh, T. L. Francis, T. S. Sreena, *Mater. Lett.* **2016**, *170*, 196.
[38] S. Hu, X. Qin, G. Zhou, X. Liu, C. Lu, Z. Xu, S. Wang, *J. Alloys Compd.* **2016**, *664*, 304.
[39] X.-Y. Sun, J.-C. Zhang, X.-G. Liu, L.-W. Lin, *Ceram. Int.* **2012**, *38*, 1065.
[40] C.-C. Wu, K.-B. Chen, C.-S. Lee, T.-M. Chen, B.-M. Cheng, *Chem. Mater.* **2007**, *19*, 3278.
[41] Y. Zheng, H. You, G. Jia, K. Liu, Y. Song, M. Yang, H. Zhang, *Cryst. Growth Des.* **2009**, *9*, 5101.
[42] Y. Tian, B. Chen, B. Tian, Y. Mao, J. Sun, X. Li, J. Zhang, S. Fu, H. Zhong, B. Dong, X. Zhang, H. Xia, R. Hua, *J. Nanopart. Res.* **2013**, *15*, 1757.
[43] N. O. Nuñez, S. Rivera, D. Alcantara, J. M. de la Fuente, J. García-Sevillano, M. Ocaña, *Dalton Trans.* **2013**, *42*, 10725.
[44] Y. X. Yeng, M. Ghebrebrhan, P. Bermel, W. R. Chan, J. D. Joannopoulos, M. Soljačić, I. Celanovic, *Proc. Natl. Acad. Sci. USA* **2012**, *109*, 2280.
[45] R. S. Meltzer, S. P. Feofilov, B. Tissue, H. B. Yuan, *Phys. Rev. B* **1999**, *60*, R14012.
[46] J. C. Boyer, F. Vetrone, J. A. Capobianco, A. Speghini, M. Bettinelli, *J. Phys. Chem. B* **2004**, *108*, 20137.
[47] T. Senden, F. T. Raouw, A. Meijerink, *ACS Nano* **2015**, *9*, 1801.
[48] L. Novotny, B. Hecht, *Principles of Nano Optics*, Cambridge University Press, New York **2006**.
[49] S. Colodrero, M. Ocaña, A. R. González-Elipe, H. Míguez, *Langmuir* **2008**, *24*, 9139.
[50] A. Jiménez-Solano, J. Galisteo-López, H. Míguez, *Small* **2015**, *11*, 2727.
[51] A. Zelcer, G. J. A. A. Soler-Illia, *J. Mater. Chem. C* **2013**, *1*, 1359.
[52] J. R. Castro Smirnov, M. E. Calvo, H. Míguez, *Adv. Funct. Mater.* **2013**, *23*, 2805.